

Surface Energy-Mediated Self-Catalyzed CsPbBr₃ Nanowires for Phototransistors

Dengji Li, You Meng, Yini Zheng, Pengshan Xie, Xiaolin Kang, Zhengxun Lai, Xiuming Bu, Wei Wang, Weijun Wang, Furong Chen, Chuntai Liu, Changyong Lan, SenPo Yip, and Johnny C. Ho*

Controllable self-catalyzed growth of semiconductor nanowires (NWs) is of great importance, particularly to avoid impurities coming from foreign catalysts to deteriorate the NW properties. Although this catalyst-free NW growth has many obvious advantages, there are very limited works focused on all-inorganic CsPbBr₃ perovskite NWs, which is one of the recent champion materials for electronics and optoelectronics. Here, a direct self-catalyzed synthesis of freestanding CsPbBr₃ NWs via vapor–liquid–solid growth mechanism by chemical vapor deposition is developed. Notably, manipulation of the substrate surface roughness is the key enabling parameter for the self-catalyzed NW growth here. It is revealed that the surface energy of substrates, modulated by its surface roughness, is found to effectively mediate the self-catalytic growth of CsPbBr₃ NWs. When configured into photodetectors, the intrinsic p-type CsPbBr₃ NWs exhibit good optoelectronic performance with a photoresponsivity of $\approx 2000 \text{ A W}^{-1}$, a detectivity of $\approx 2.57 \times 10^{12}$ Jones, and a fast response down to 362 μs . All these results evidently indicate the technological potential of this self-catalyzed synthesizing route for other high-quality all-inorganic perovskite NWs.

optoelectronics.^[1] To date, CsPbX₃ perovskites have been successfully fabricated in various nanoscale morphologies, such as nanocrystals, nanoplates, nano/micro-rods, nanowires (NWs), and quantum dots, in which their properties are widely explored.^[2] Particularly, 1D CsPbX₃ NWs are discovered to provide unique charge transport pathways along the axial direction together with many intriguing characteristics, including good elasticity,^[3] flexibility,^[4] ductility,^[5] transparency,^[6] and polarization-sensitive,^[7] suggesting their versatile technological potency for various utilization.

At the same time, among various synthesis methods, although several solution-phase techniques have been realized to synthesize perovskites, when they come to CsPbX₃ NWs, the poor crystalline quality and high surface defect density of the obtained products would greatly limit the further development.^[8] By contrast, vapor-

phase methods have been demonstrated as an efficient alternative pathway to grow high-quality CsPbX₃ NWs. With enormous efforts being adopted, precise control of growth conditions are found to effectively regulate the morphology, crystallinity, and composition of the products.^[9] For instance, the higher level control in growth is achieved through the introduction of van

1. Introduction

In recent years, due to the strong light absorption, long carrier lifetime, tunable bandgap, and robust stability, all-inorganic lead halide perovskites (CsPbX₃; X = Cl, Br, or I) have attracted extensive research attention for next-generation electronics and

D. J. Li, Y. Meng, Y. N. Zheng, P. S. Xie, X. L. Kang, Z. X. Lai, X. M. Bu, W. Wang, W. J. Wang, F. R. Chen
Department of Materials Science and Engineering
City University of Hong Kong
Kowloon, Hong Kong SAR 999077, P. R. China

C. T. Liu
Key Laboratory of Advanced Materials Processing
& Mold (Zhengzhou University)
Ministry of Education
Zhengzhou 450 002, P. R. China

C. Y. Lan
State Key Laboratory of Electronic Thin Films and Integrated Devices
University of Electronic Science and Technology of China
Chengdu 610 054, P. R. China

S. P. Yip, J. C. Ho
Institute for Materials Chemistry and Engineering
Kyushu University
Fukuoka 816 8580, Japan

J. C. Ho
Department of Materials Science and Engineering
State Key Laboratory of Terahertz and Millimeter
Waves, and Hong Kong Institute for Advanced Study
City University of Hong Kong
Kowloon, Hong Kong SAR 999077, P. R. China
E-mail: johnnyho@cityu.edu.hk

 The ORCID identification number(s) for the author(s) of this article can be found under <https://doi.org/10.1002/aelm.202200727>.

DOI: 10.1002/aelm.202200727

der Waals (vdW) epitaxial growth,^[10] graphoepitaxial effect,^[11] template-assisted growth,^[12] and substrate surface roughness.^[13] More interesting, high-quality NWs were vertically grown on substrates with the assistance of Tin (Sn) particle catalysts through vapor–liquid–solid (VLS) mechanism.^[14] These vertically grown CsPbX₃ NWs provide tremendous convenience for the further material characterization, device fabrication and integration. However, the Sn catalysts would inevitably introduce impurity atoms to CsPbBr₃ NWs and thus altering their intrinsic material properties; hence, it is essential to enhance the manufacture route to gain high-purity perovskite NWs.

Generally, the VLS NW growth relies on a liquid metal catalyst to achieve the self-assembly of semiconductor nanostructures and to stabilize the growth.^[15] It has been reported that the special VLS growth could also occur without introducing foreign metal as catalytic seeds in III-V NW growth, which is known as the “self-catalyzed” process.^[16] For instance, the source Ga can act directly as the liquid catalyst to synthesize GaAs NWs.^[17] Since the contamination issues related to the foreign impurity atoms are avoided, this manufacturing route gains intense attention in recent years for the cutting-edge studies.^[18] Inspired by this idea, changing the foreign metal catalytic seeds to self-catalytic seeds may be a promising strategy to improve the VLS growth process of perovskites.

Here, we explore a direct self-catalyzed VLS synthesis route for high-quality freestanding CsPbBr₃ NWs on SiO₂/Si substrates. Through modifying the roughness of substrates, the Pb flux dissolved from the evaporated PbBr₂ source will aggregate spontaneously into Pb droplets and act as the key catalytic seeds. This growth process of CsPbBr₃ NWs is highly similar to the established self-catalyzed VLS model of group III-V materials.^[16] Besides, the surface energy of substrates is found to effectively mediate the growth of CsPbBr₃ NWs. When configured into phototransistors, the self-catalyzed CsPbBr₃ NWs exhibit intrinsic p-type properties and comparable optoelectronic performance with state-of-the-art NW devices. All these results suggest the technological potency of these high-purity freestanding CsPbBr₃ NWs for various electronic applications.

2. Results and Discussion

In this work, the freestanding CsPbBr₃ perovskite NWs were grown on surface-roughened SiO₂/Si substrates (50 nm thick thermal oxide) via the chemical vapor deposition (CVD) process in a two-zone tube furnace. A mixture of PbBr₂ and CsBr powders with 2:1 molar ratio was grinded and placed at the center of the upstream heating zone of a quartz tube. Before the growth, the roughened substrate was prepared by controlled scratching process and positioned in the downstream heating zone, which is ≈15 cm away from the precursor powders. Meanwhile, 100 sccm of high-purity argon gas was injected into the CVD system, with the pressure kept at 1.5 Torr. During the growth process, the upstream heating zone was heated up to 480 °C and held at that temperature for 20 min, while the downstream zone was set to the similar process with heating temperature of 330 °C. After deposition, the entire system was naturally cooled to room temperature and a mass of orange and yellow products were obtained on the substrates. The growth system is also schematically

shown in Figure S1 (Supporting Information) with more details of the NW growth provided in the Experimental Section.

After the growth, scanning electron microscopy (SEM) was adopted to evaluate the morphology of as-grown NWs. As shown in **Figure 1a**, vertical NWs are readily fabricated on the surface-roughened substrate, whereas almost all the NWs are grown along the “scratched” lines. On the contrary, as depicted in the inset image, bulk clusters are only formed on the smooth substrate under the same growth condition. Notably, the obtained NWs are straight and smooth with an obvious spherical shape at the tip, designating the self-catalyzed VLS growth process here (Figure 1b). The top-view and cross-sectional view SEM images are also provided in Figure S2 (Supporting Information). We then performed the energy-dispersive X-ray spectroscopy (EDS) mapping to achieve the elemental analysis (Figure 1c), from which Cs, Pb, and Br are uniformly distributed along the NW body. Besides, the EDS spectrum indicates that the composition ratio of Cs, Pb, Br is close to 1:1:3 (Figure S3, Supporting Information), agreeing well with the stoichiometric ratio of CsPbBr₃. Meanwhile, the influence of gas pressure and location of substrate to the NW growth was also investigated. As presented in Figure S4 (Supporting Information), when the gas pressure is increased, the nucleation density of bulk clusters would decrease obviously; and when distance between substrate and precursor is increased, the nucleation density of bulk clusters would decrease dramatically and the NWs formed on the scratched lines would be more remarkable.

Next, in order to investigate the crystal quality and phase purity of our self-catalyzed NWs, powder X-ray diffraction (XRD), photoluminescence (PL), X-ray photoelectron spectroscopy (XPS), and transmission electron microscopy (TEM) were employed. Figure 1d shows the diffraction peaks of as-fabricated NWs, where all the peaks are clearly indexed to monoclinic CsPbBr₃ (JCPDS #18-0364). Figure 1e depicts the PL spectrum of our NWs, in which a sharp characteristic emission peak is observed at about 540 nm, being consistent with that of monoclinic CsPbBr₃ NWs.^[11] Also, as displayed in the XPS spectra in Figure S5 (Supporting Information), all the peaks of Cs 3d_{5/2}, Cs 3d_{3/2}, Pb 4f_{7/2}, Pb 4f_{5/2}, Br 3d_{5/2}, and Br 3d_{3/2} can be well identified, while no impurity associated peaks are detected. All these results evidently suggest that the crystalline and phase-pure NWs are obtained in our self-catalytic perovskite NW growth.

At the same time, transmission electron microscopy (TEM) and selected-area electron diffraction (SAED) were utilized to further evaluate the crystallinity of self-catalyzed NWs. As shown in Figure 1f, the diameter of a representative NW is around 90 nm, while its surface is very smooth. The diameter distribution of the CsPbBr₃ NWs grown on surface-roughened substrate was assessed from the TEM images and illustrated in **Figure 2g**. The corresponding length distribution was provided in Figure S9 (Supporting Information). When the high resolution mode was applied, clear lattice fringes were observed in Figure 1g, which infers the single-crystalline nature of NW without any impurity phase. The spacing between two adjacent lattice planes is found to be 0.58 nm, which corresponds to the (100) plane of monoclinic CsPbBr₃ (Figure 1h). The corresponding SAED pattern confirms that the NW is grown along the [100] direction (Figure 1i), agreeing perfectly with the

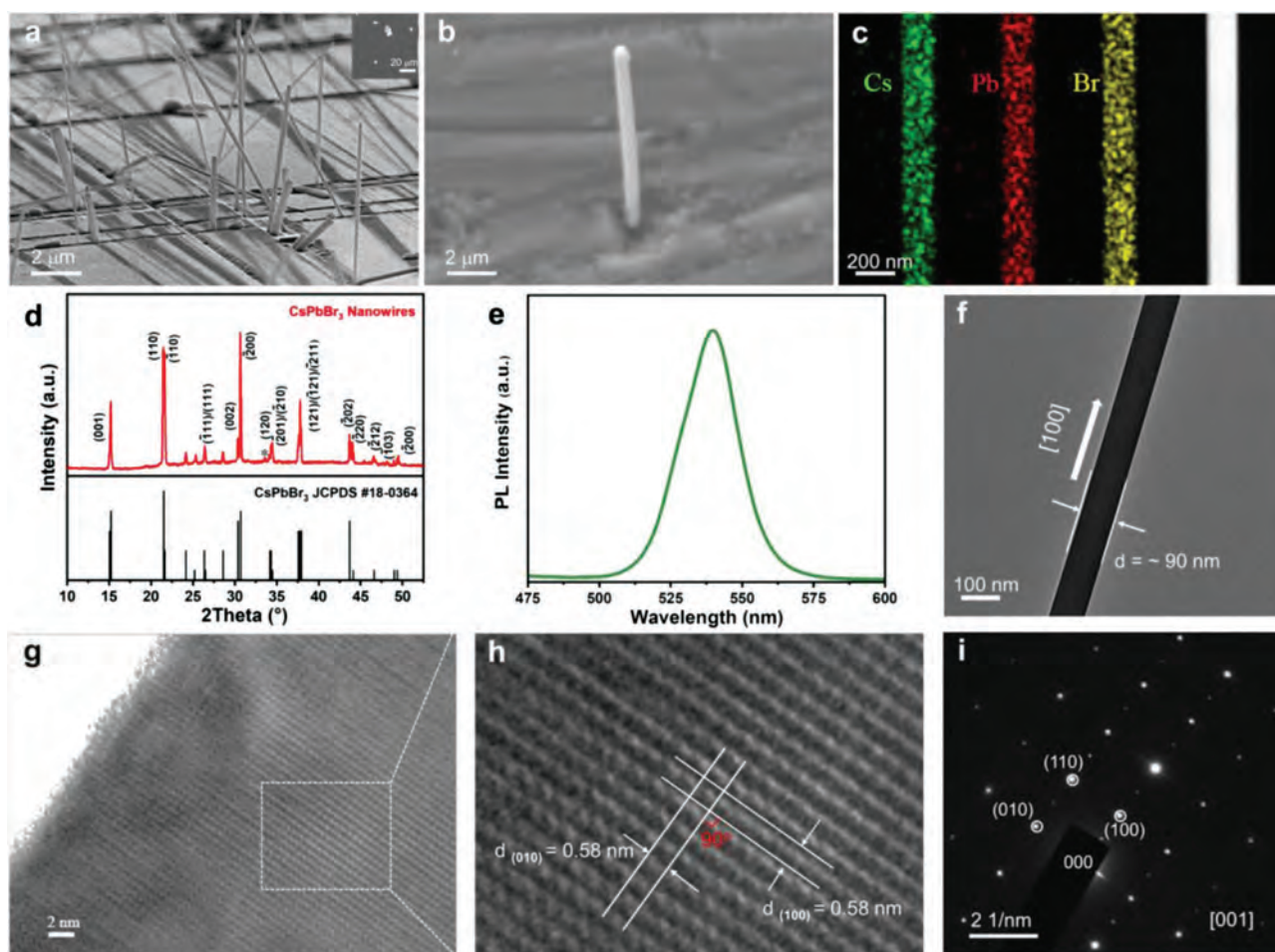


Figure 1. Characterization of the self-catalyzed CsPbBr₃ NWs. a) SEM image of self-catalyzed CsPbBr₃ NWs grown on the surface-roughened SiO₂/Si substrate. Inset shows the products grown on smooth SiO₂/Si substrates. b) High-resolution SEM image of a typical CsPbBr₃ NW vertically grown on the “scratched” point. c) EDS elemental mapping showing Cs (green), Pb (red), and Br (yellow) and the corresponding high-angle dark-field STEM image. d) X-ray diffraction spectrum, e) normalized PL spectrum, f) TEM image of the self-catalyzed CsPbBr₃ NWs. g,h) HRTEM images of the CsPbBr₃ NW body and i) the corresponding SAED pattern.

high-resolution TEM (HRTEM) result. It is worth mentioning that hundreds of NWs have also been characterized with the same process, and almost all of them exhibit the same growth orientation of [100]. This particular growth orientation is as well widely reported in other CsPbBr₃ works as its surface free energy of (100) plane is calculated to be lower than that of other crystal planes.^[19]

To shed light on the impact of substrate surface roughness on the growth of vertical NWs, the surface morphology of SiO₂/Si substrates with different surface roughness were studied by atomic force microscopy (AFM). For the initial smooth substrate, as shown in **Figure 3a**, the peak height is up to 10 nm and the root-mean-square (RMS) roughness is measured to be 0.2 nm. Once the substrate is controllably scratched by sandpaper (1200 mesh), scratch lines are clearly witnessed on the surface with the peak height close to 914.2 nm and the RMS roughness of 84.7 nm (Figure 3b). For the surface-roughened substrate processed with 400 mesh sandpaper, the height region comes to a range of −1.6 to 0.7 μm (Figure S6a, Supporting Information). Control experiments of NW growth were

then performed on the SiO₂/Si substrates with and without the scratching process. As shown in Figures S6b and S7 (Supporting Information), the formation of NWs is distinctly less in the un-scratched substrate as compared with that in the scratched substrate.

In this case, it is important to understand the relationship between NW growth and substrate feature. Here, we performed the contact angle measurement on SiO₂/Si substrates with and without the scratching process. The contact angle characterization is chosen because it can provide quantitative data about surface energy of different substrates. According to the Young's equation,^[21] the contact angle (θ) between flat substrate and water droplet satisfy the relationship of $\gamma_s = \gamma_L \cos\theta + \gamma_{sL}$, in which γ_s , γ_L and γ_{sL} are the surface energy of solid substrate, the surface tension of liquid droplet, and the interfacial tension between liquid and solid, respectively. From the images presented in Figure 3a,b, the scratched substrate possesses a smaller contact angle of 30° than that of the smooth substrate of 50°. This phenomenon represents that the scratching process could increase the surface energy of SiO₂ substrate, and

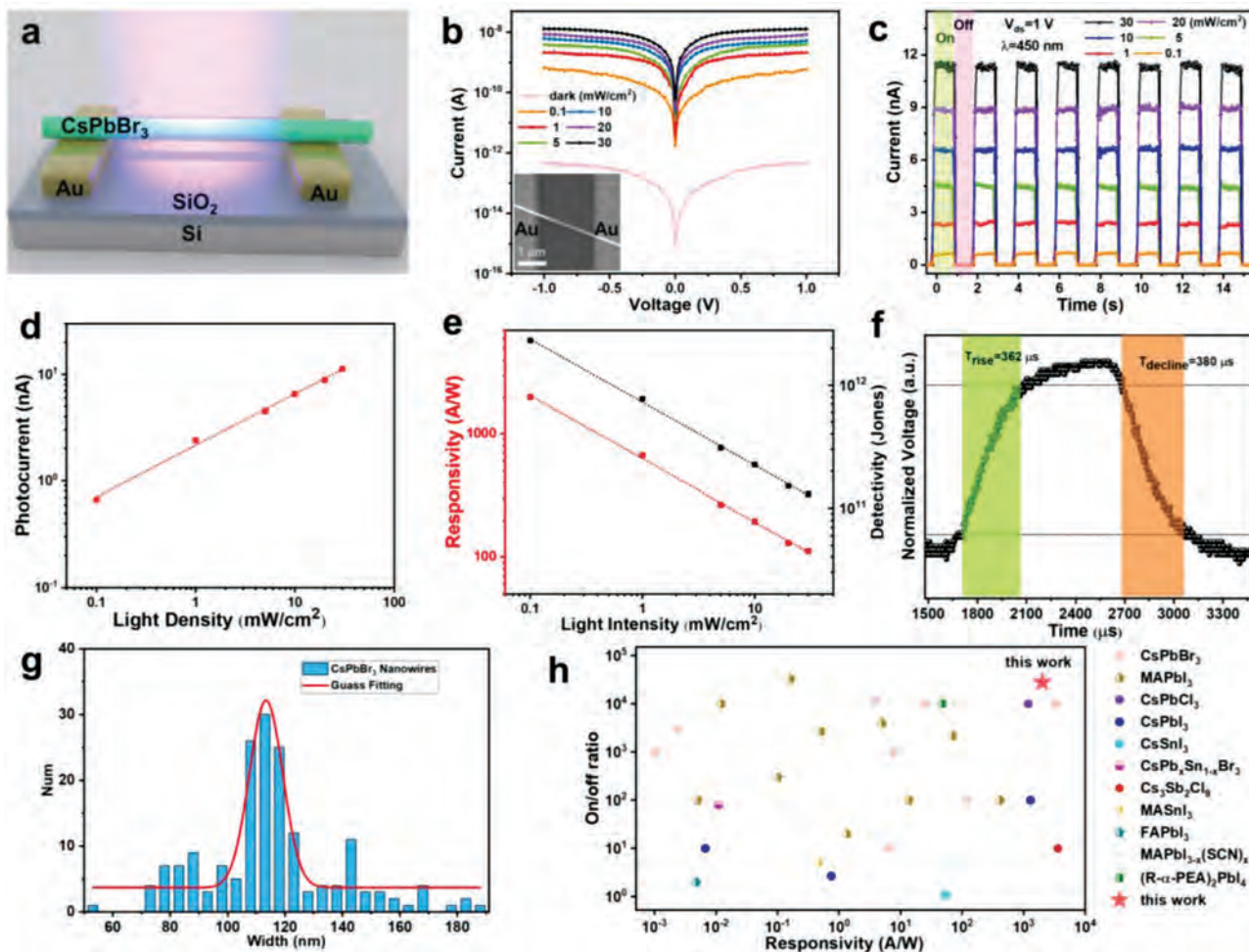


Figure 2. Characterization of the self-catalyzed CsPbBr₃ NW photodetector. a) Schematic illustration of the photodetector based on a single CsPbBr₃ NW. b) *I*–*V* curves with and without light irradiation. Inset shows the SEM image of the device. c) Time-resolved photoresponse of the device under different light illumination. Drain voltage is 1 V. d) Photocurrent, e) responsivity, and detectivity as a function of light intensity. f) Rise and decay times of the photodetector. g) Diameter statistics of the CsPbBr₃ NWs grown on surface-roughened substrate. h) Performance comparison among our self-catalyzed CsPbBr₃ NWs and other reported perovskite NWs (detailed performance parameters are provided in Tables S1 and S2, Supporting Information).

later enhance the NW nucleation density on its surface. Our observation are consistent to the theoretical and experimental works reported previously,^[22] in which the samples prefer to nucleate on the high surface energy area (Figure S7, Supporting Information).

After that, it is crucial to incorporate the effect of substrate surface roughness into the investigation of growth kinetics of our vertical perovskite NWs. At first, HRTEM images are taken on the NW tip region, where a characteristic spherical seed is evidently observed (Figure 3d), confirming the VLS growth process here. More importantly, the lattice fringes and corresponding diffraction patterns are also collected from the tip (Figure 3e,f), revealing the existence of the catalytic PbBr₂ seed. Recently, two-step growth of the CsPbX₃ perovskite NWs was reported through the chemical conversion of PbX₂ to perovskites.^[9a,23] However, these two-step converted perovskite NWs exhibit distorted NW surfaces and disordered orientation, since the chemical conversion process would inevitably induce volume expansion and uncontrolled strain during the formation of NWs.^[9a] This defective phenomenon is not found in our

one-step CsPbBr₃ NW growth, also highlighting the unique self-catalytic growth process in this study.

Furthermore, it is necessary to evaluate the growth mechanism of these vertical CsPbBr₃ NWs, in which a one-step self-catalytic VLS mechanism is proposed. Based on the previous works on III-V NWs,^[24] the vital point of the VLS growth is the formation of catalytic liquid droplets. Special attention needs to be given to the accommodation of the arriving source from the precursors. Since the melting point of CsBr (636 °C) is much higher than that of PbBr₂ (373 °C), PbBr₂ will be first evaporated from precursor prior to CsBr.^[9a,25] After the gas source comes into zone II (the substrate zone) with the flow of argon, the gas source will nucleate preferably at the high surface energy area on substrates due to the decline of temperature. Simultaneously, the scratched lines are proven to have a higher surface energy compared to the smooth area, being preferable sites for the formation of Pb droplets. Because Pb has a relatively low melting point of 327.4 °C;^[26] Pb species would get deposited onto the substrate as liquid droplets (Figure 4a). In this case, the liquid droplets act as active sites for the catalytic

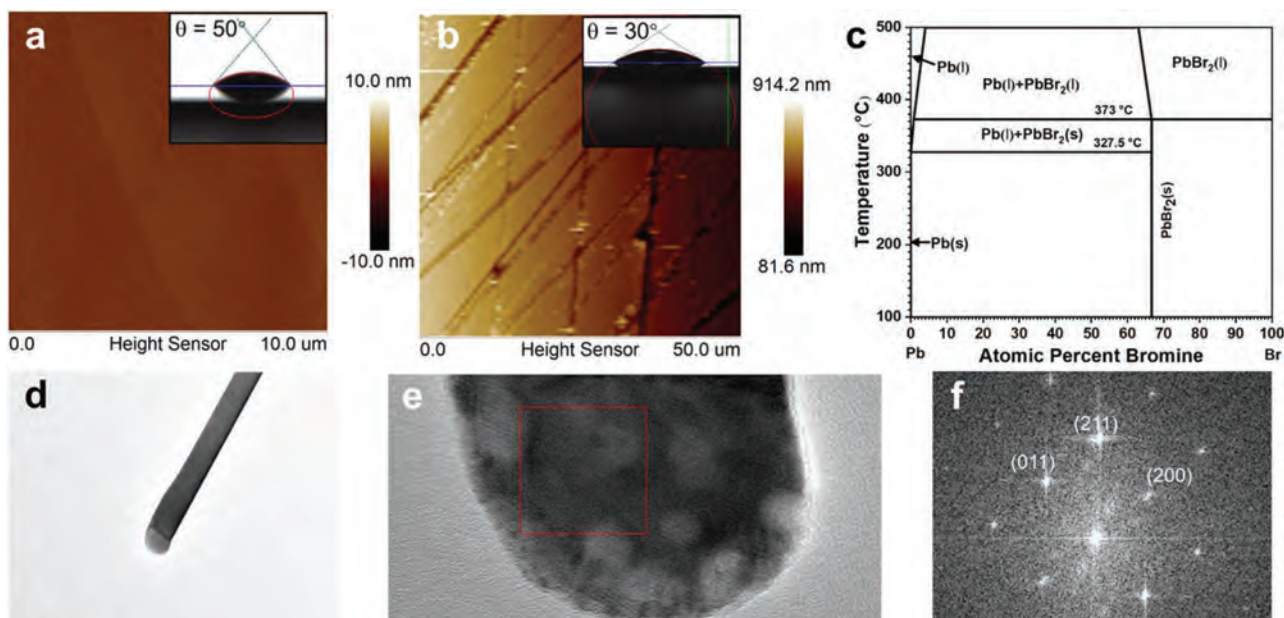


Figure 3. Characterization of the substrate surface and tip region of grown NWs. a) AFM image of the smooth SiO₂/Si substrate. Inset illustrates the corresponding water contact angle on the surface. b) AFM image of the surface-roughened substrate. Inset shows the corresponding water contact angle on the surface. c) Phase diagram of the Pb-Br alloy.^[20] d,e) HRTEM images of the tip of a typical CsPbBr₃ NW. f) Corresponding SAED pattern of the NW tip.

nucleation of NWs. According to the phase diagram of PbBr₂ (Figure 3c), the droplet would gradually become supersaturated with the continuous absorption of Br₂. Therefore, the alloyed droplets function as the intermediate catalysts to nucleate and form the PbBr_x solid seeds (Figure 4b). When the source temperature increases, CsBr starts to evaporate and flow into the substrate zone with the assistance of argon carrier gas. Once the PbBr_x droplets become activated, the Cs-containing species would be adsorbed onto the surface of the droplets and react with PbBr_x seeds. As the perovskite CsPbBr₃ structure has the relatively low formation energy and stable crystal structure, the supersaturated CsPbBr₃ NWs are eventually grown in the vertical manner (Figure 4c).^[14]

Apart from understanding the growth of self-catalyzed NWs, it is also important to study their photoelectric performance. Taking advantage of the high quality and vertical growth of self-catalyzed CsPbBr₃ NWs, a single NW photodetector device was fabricated through the dry-transfer method (with detailed fabrication procedures provided in the Experimental Section). In brief, Au electrodes with a thickness of 50 nm and a channel length of 2 μm were prefabricated by standard lithography and metallization on SiO₂/Si substrates. Figure 2a shows the schematic diagram of the device, whereas a 450 nm light source is adopted to illuminate the device. The corresponding current–voltage (*I*–*V*) curves are measured in the dark and under different light intensities (0.1–30 mW cm⁻²) as shown in Figure 2b. It is seen that the single NW device has a dark current down to fA level. Meanwhile, under 0.1 mW cm⁻² illumination, the output current increases by about 4 orders of magnitude to above 10 nA. It can also be observed that the photocurrent is proportional to the drain voltage and illumination intensity. The symmetrical shape of the curve confirms that there is not significant resistance between Au and NW, revealing a good electrical contact for carrier collection.

More importantly, all fabricated photodetector devices based on self-catalyzed CsPbBr₃ NWs exhibit good stability and reliability, as there is not any noticeable degradation during repeated on/off switching cycles (Figure 2c). Next, we focus on the photocurrent (*I*_p = *I*_{light} – *I*_{dark}) versus light intensity (*P*) plot, their relation is found to well satisfy the equation of *I*_p = *A**P*^{*k*}, where *A* and *k* are the empirical parameters.^[27] The parameter *k* is estimated to be 0.5 through linear fitting. This sublinear relationship is often observed in semiconductor NW based photodetectors, which is owing to the complicated process of trap filling, energy band bending, carrier generation, trapping, and recombination.^[28]

One of the most vital figures of merit for a photodetector is its photoresponsivity, *R*, which is defined as

$$R = \frac{I_{\text{light}}}{PS} \quad (1)$$

where *S* is the actual illuminated area. Meanwhile, another important figures of merit parameter to quantify the performance of devices is detectivity (*D*^{*}), which is defined as

$$D^* = R \cdot \sqrt{\frac{S}{2eI_{\text{dark}}}} \quad (2)$$

where *e* is the electronic charge. As depicted in Figure 2e, both *R* and *D*^{*} decrease dramatically with the increasing light intensity. This reduction trend in photoresponsivity and detectivity may be explained in terms of the trap states existed either at the interface between CsPbBr₃ NW and underlying SiO₂ layer or within the NW.^[29] At a relatively low illumination intensity (0.1 mW cm⁻²), our device reaches a high photoresponsivity of 2006 A W⁻¹ and a good detectivity of 2.57 × 10¹² Jones, being comparable to the state-of-the-art perovskite NW based photodetectors. In order to precisely measure the response time, a

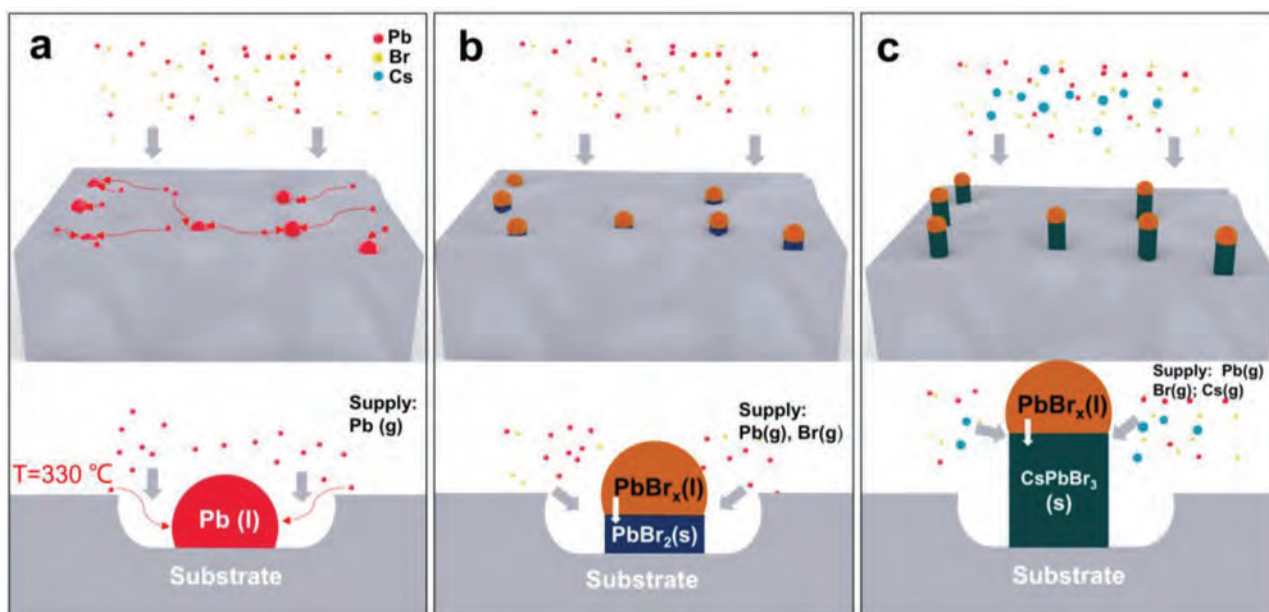


Figure 4. Schematic illustration of different growth stages of the freestanding CsPbBr₃ NWs. a) Formation of large Pb droplets on the surface-roughened substrate. b) Growth of PbBr₂ NW seeds. c) Growth of CsPbBr₃ NWs.

high frequency chopper was adopted to modulate the on and off states of illumination, and a digital oscilloscope was utilized to record the high-resolution photoresponse. As presented in Figure 2e, the rise (green area) and decay (red area) times, defined as the time for the photocurrent to vary from 10% to 90% of the peak current and from 90% to 10% of the peak current, are measured to be 362 and 380 μ s, respectively. The detailed performance comparison among light/dark current ratio and responsivity of photodetectors based on perovskite NWs reported previously is compiled in the Figure 2h, which suggests the excellent photodetection performance of our self-catalyzed CsPbBr₃ NWs.

Furthermore, the phototransistor based on a single CsPbBr₃ NW with a bottom-gate top-contact structure was fabricated and thoroughly studied (Figure S10, Supporting Information). The degenerately p-doped Si is employed as a bottom gate while the 280 nm thick thermal oxide is used as the dielectric layer. After the CsPbBr₃ NW is dry-transferred onto the SiO₂/Si

substrate (the dry-transfer result shown in Figure S8, Supporting Information), a shadow mask is adopted to deposit the patterned Au electrode. The channel length is designed as 20 μ m and the evaporated Au electrode is \approx 50 nm thick. The device shows the typical p-type semiconducting behavior with a field-effect hole mobility estimated of \approx 0.05 cm² V⁻¹ s⁻¹ (Figure 5a). The transfer curves with a constant drain voltage of 5 V and gate voltages switching from 40 to -40 V in both dark and illumination conditions were recorded. Without illumination, the CsPbBr₃ NW transistor exhibited an on/off current ratio of 10⁴, while the irradiation can effectively elevate the source-drain current under the same gate bias (Figure 5b,c). Output characteristics of additional devices are shown in Figure S11 (Supporting Information). Besides, the performance comparison of the top-contact (20 μ m channel length) and bottom-contact (2 μ m channel length) photodetector devices is shown in Figure S12 (Supporting Information). In future, other enhancement techniques, such as controllable foreign atom

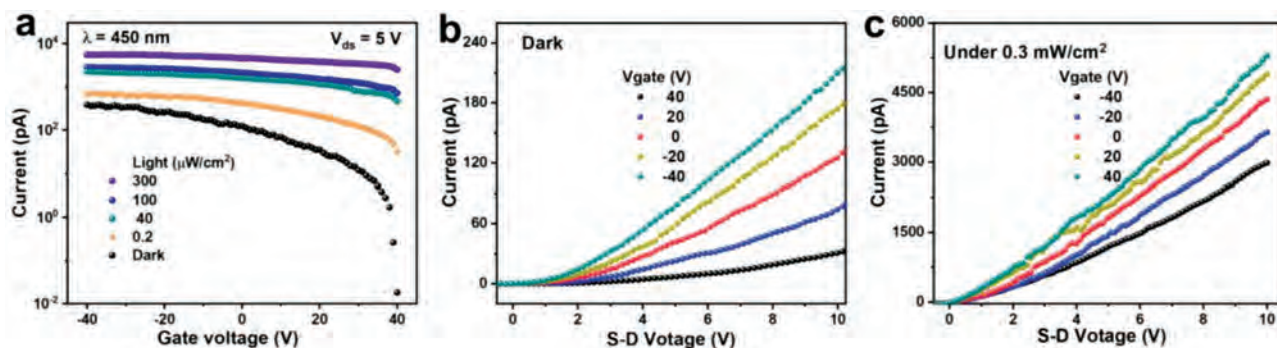


Figure 5. Characterization of self-catalyzed CsPbBr₃ single NW FETs. a) Transfer characteristics of the CsPbBr₃ single NW FETs with and without light illumination. Corresponding output curves measured in the dark b) and c) under 0.3 mW cm⁻² illumination.

doping and charge transfer doping, can be applied to further enhance the device performance of our self-catalyzed CsPbBr₃ NW devices.

3. Conclusions

In summary, large-scale synthesis of vertical CsPbBr₃ NWs is successfully achieved through a self-catalyzed VLS process. The as-grown CsPbBr₃ NWs exhibit single-crystalline nature with smooth surface. Surface energy was proposed to mediate the controllable growth of self-catalyzed CsPbBr₃ NWs on substrates with different surface roughness. As for optoelectronic characteristics, individual CsPbBr₃ NW is configured into photodetectors, exhibiting a decent performance with an on/off current ratio of 2.8×10^4 , a responsivity of 2006 A W^{-1} , a detectivity of 2.57×10^{12} Jones, and a fast response time down to 362 μs . Meanwhile, the self-catalyzed intrinsically p-type NWs exhibit promising potential in the applications for phototransistors, in which their properties can be tuned by light and bias simultaneously. All these findings show the potential of our self-catalyzed CsPbBr₃ NWs for various technological utilization.

4. Experimental Section

Materials Preparation: All chemical sources used in the work were purchased from Sigma-Aldrich without any further purification process. The commercial p-type Si wafer, with a 50 nm thick thermal oxide layer, was used as the smooth substrate. The scratched substrate was surface-roughened by the 1200 and 400 mesh sandpapers. Before use, all the growth substrates were ultrasonically cleaned with pure deionized water, ethanol, and acetone, and blow-dried through a nitrogen gun. Source powder was prepared by mixing 100 mg of PbBr₂ powder and 70 mg of CsBr powder in an agate mortar and then grinded for 15 min. After that, the well-mixed source powder was annealed at 420 °C for 30 min at atmosphere before being placed into the tube furnace to suppress the evaporation process of precursors.^[30]

Synthesis of CsPbBr₃ NWs: In this work, the CsPbBr₃ NWs were fabricated in a two-zone CVD system. The prepared source powder was placed in the center of the first heating zone. The scratched SiO₂/Si wafer was placed in the downstream side of the quartz tube, which was ≈ 15 cm away from the precursor powder. After that, the CVD system was evacuated to a base pressure of 8 mTorr and then 100 sccm Ar gas was released to flow through the tube furnace. The eventual growth pressure was regulated to 1.5 Torr. Then, the first heating zone was set to heat up slowly to 480 °C in 50 min and keep at that temperature for 20 min, while the second heating zone was set to 330 °C with the same procedure. The heating temperature of source powder is 480 °C, lower to its melting point (e.g., CsBr of 636 °C); therefore, a sublimation process is happened here to generate the vapor source.

Material Characterization: The morphology of NWs was evaluated by using scanning electron microscope (SEM, quanta 450 FEG, FEI) and transmission electron microscope (TEM, Philips CM20). The crystalline structure was initially determined by the X-ray diffraction pattern (D2 Phaser Cu K α radiation, Bruker), and further verified through the high-resolution transmission electron microscopy (HRTEM, JEOL 2100F). The elemental analysis was carried out using the energy dispersive X-ray (EDX) detector connected with JEOL 2100F. The photoluminescent property of the NWs was tested by photoluminescence spectroscopy (iHR320) with an excitation wavelength of 400 nm. As for the scratched substrate, an atomic force microscopy (Bruker Dimension Icon AFM) was employed to check its surface morphologies.

Device Fabrication: The photodetectors based on single CsPbBr₃ NWs were prepared by dry transfer of NWs on a processed substrate with Au

electrodes (50 nm thick) prefabricated with a channel length of 2 μm . The Au electrodes were constructed by standard lithography and metallization on the substrate surface (50 nm thick SiO₂/Si). A standard electrical probe station connected to a semiconductor analyzer (Agilent 4155C) was utilized to assess the electrical property of the NWs. Laser diodes of 405 nm were used as the light source for the photodetection measurement. A PM400 power meter (Thorlabs) was used to detect the power of the incident irradiation. The TBS 1102B-EDU digital oscilloscope (Tektronix) was connected with a SR570 current preamplifier (Stanford Research Systems) to measure the high-precision photoresponse speed.

Supporting Information

Supporting Information is available from the Wiley Online Library or from the author.

Acknowledgements

This research was financially supported by a fellowship award from the Research Grants Council of the Hong Kong Special Administrative Region, China (CityU RFS2021-1S04).

Conflict of Interest

The authors declare no conflict of interest.

Data Availability Statement

The data that support the findings of this study are available from the corresponding author upon reasonable request.

Keywords

all-inorganic perovskites, nanowires, photodetectors, phototransistors, self-catalyzed growth

Received: June 28, 2022
Revised: September 1, 2022
Published online: September 20, 2022

- [1] a) M. Kulbak, S. Gupta, N. Kedem, I. Levine, T. Bendikov, G. Hodes, D. Cahen, *J. Phys. Chem. Lett.* **2016**, *7*, 167; b) M. Kulbak, D. Cahen, G. Hodes, *J. Phys. Chem. Lett.* **2015**, *6*, 2452; c) H. Zhu, Y. Fu, F. Meng, X. Wu, Z. Gong, Q. Ding, M. V. Gustafsson, M. T. Trinh, S. Jin, X. Y. Zhu, *Nat. Mater.* **2015**, *14*, 636; d) L. N. Quan, R. Quintero-Bermudez, O. Voznyy, G. Walters, A. Jain, J. Z. Fan, X. Zheng, Z. Yang, E. H. Sargent, *Adv. Mater.* **2017**, *29*, 1605945; e) J. Li, L. Xu, T. Wang, J. Song, J. Chen, J. Xue, Y. Dong, B. Cai, Q. Shan, B. Han, H. Zeng, *Adv. Mater.* **2017**, *29*, 1603885; f) Q. Zhang, R. Su, W. Du, X. Liu, L. Zhao, S. T. Ha, Q. Xiong, *Small Methods* **2017**, *1*, 1700163; g) D. Zhang, Y. Yang, Y. Bekenstein, Y. Yu, N. A. Gibson, A. B. Wong, S. W. Eaton, N. Kornienko, Q. Kong, M. Lai, A. P. Alivisatos, S. R. Leone, P. Yang, *J. Am. Chem. Soc.* **2016**, *138*, 7236; h) Y. Bekenstein, B. A. Koscher, S. W. Eaton, P. Yang, A. P. Alivisatos, *J. Am. Chem. Soc.* **2015**, *137*, 16008.
- [2] a) D. Zhang, S. W. Eaton, Y. Yu, L. Dou, P. Yang, *J. Am. Chem. Soc.* **2015**, *137*, 9230; b) G. Raino, M. A. Becker, M. I. Bodnarchuk, R. F. Mahrt, M. V. Kovalenko, T. Stoferle, *Nature* **2018**, *563*, 671;

- c) X. Hu, H. Zhou, Z. Jiang, X. Wang, S. Yuan, J. Lan, Y. Fu, X. Zhang, W. Zheng, X. Wang, X. Zhu, L. Liao, G. Xu, S. Jin, A. Pan, *ACS Nano* **2017**, *11*, 9869; d) X. Wang, H. Zhou, S. Yuan, W. Zheng, Y. Jiang, X. Zhuang, H. Liu, Q. Zhang, X. Zhu, X. Wang, A. Pan, *Nano Res.* **2017**, *10*, 3385; e) D. Yang, X. Li, W. Zhou, S. Zhang, C. Meng, Y. Wu, Y. Wang, H. Zeng, *Adv. Mater.* **2019**, *31*, 1900767.
- [3] X. Li, Y. Meng, R. Fan, S. Fan, C. Dang, X. Feng, J. C. Ho, Y. Lu, *Nano Res.* **2021**, *14*, 4033.
- [4] M. A. Reyes-Martinez, A. L. Abdelhady, M. I. Saidaminov, D. Y. Chung, O. M. Bakr, M. G. Kanatzidis, W. O. Soboyejo, Y. L. Loo, *Adv. Mater.* **2017**, *29*, 1606556.
- [5] C. Zhao, Y. Liu, L. Chen, J. Li, H. Y. Fu, S. Zhao, W.-D. Li, G. Wei, *ACS Appl. Electron. Mater.* **2020**, *3*, 337.
- [6] Q. Shang, C. Li, S. Zhang, Y. Liang, Z. Liu, X. Liu, Q. Zhang, *Nano Lett.* **2020**, *20*, 1023.
- [7] X. Wang, Y. Wang, W. Gao, L. Song, C. Ran, Y. Chen, W. Huang, *Adv. Mater.* **2021**, *33*, 2003615.
- [8] a) K. Park, J. W. Lee, J. D. Kim, N. S. Han, D. M. Jang, S. Jeong, J. Park, J. K. Song, *J. Phys. Chem. Lett.* **2016**, *7*, 3703; b) J. H. Im, J. Luo, M. Franckevicius, N. Pellet, P. Gao, T. Moehl, S. M. Zakeeruddin, M. K. Nazeeruddin, M. Gratzel, N. G. Park, *Nano Lett.* **2015**, *15*, 2120; c) L. Gu, M. M. Tavakoli, D. Zhang, Q. Zhang, A. Waleed, Y. Xiao, K. H. Tsui, Y. Lin, L. Liao, J. Wang, Z. Fan, *Adv. Mater.* **2016**, *28*, 9713.
- [9] a) J. K. Meyers, S. Kim, D. J. Hill, E. E. M. Cating, L. J. Williams, A. S. Kumbhar, J. R. McBride, J. M. Papanikolas, J. F. Cahoon, *Nano Lett.* **2017**, *17*, 7561; b) Q. Zhang, R. Su, X. Liu, J. Xing, T. C. Sum, Q. Xiong, *Adv. Funct. Mater.* **2016**, *26*, 6238; c) X. Hu, X. Wang, P. Fan, Y. Li, X. Zhang, Q. Liu, W. Zheng, G. Xu, X. Wang, X. Zhu, A. Pan, *Nano Lett.* **2018**, *18*, 3024.
- [10] J. Chen, Y. Fu, L. Samad, L. Dang, Y. Zhao, S. Shen, L. Guo, S. Jin, *Nano Lett.* **2017**, *17*, 460.
- [11] M. Shoaib, X. Zhang, X. Wang, H. Zhou, T. Xu, X. Wang, X. Hu, H. Liu, X. Fan, W. Zheng, T. Yang, S. Yang, Q. Zhang, X. Zhu, L. Sun, A. Pan, *J. Am. Chem. Soc.* **2017**, *139*, 15592.
- [12] A. Waleed, M. M. Tavakoli, L. Gu, S. Hussain, D. Zhang, S. Poddar, Z. Wang, R. Zhang, Z. Fan, *Nano Lett.* **2017**, *17*, 4951.
- [13] C. Lan, R. Dong, Z. Zhou, L. Shu, D. Li, S. Yip, J. C. Ho, *Adv. Mater.* **2017**, *29*, 1702759.
- [14] Y. Meng, C. Lan, F. Li, S. Yip, R. Wei, X. Kang, X. Bu, R. Dong, H. Zhang, J. C. Ho, *ACS Nano* **2019**, *13*, 6060.
- [15] a) N. P. Dasgupta, J. Sun, C. Liu, S. Brittman, S. C. Andrews, J. Lim, H. Gao, R. Yan, P. Yang, *Adv. Mater.* **2014**, *26*, 2137.
- [16] J. Tersoff, *Nano Lett.* **2015**, *15*, 6609.
- [17] F. Panciera, Z. Baraissov, G. Patriarche, V. G. Dubrovskii, F. Glas, L. Travers, U. Mirsaidov, J. C. Harmand, *Nano Lett.* **2020**, *20*, 1669.
- [18] a) B. Mandl, J. Stangl, E. Hilner, A. A. Zakharov, K. Hillerich, A. W. Dey, L. Samuelson, G. Bauer, K. Deppert, A. Mikkelsen, *Nano Lett.* **2010**, *10*, 4443; b) D. Rudolph, S. Hertenberger, S. Bolte, W. Paosangthong, D. Spirkoska, M. Doblinger, M. Bichler, J. J. Finley, G. Abstreiter, G. Koblmüller, *Nano Lett.* **2011**, *11*, 3848; c) X. Yu, H. Wang, J. Lu, J. Zhao, J. Misuraca, P. Xiong, S. von Molnar, *Nano Lett.* **2012**, *12*, 5436.
- [19] a) H. Zhou, S. Yuan, X. Wang, T. Xu, X. Wang, H. Li, W. Zheng, P. Fan, Y. Li, L. Sun, A. Pan, *ACS Nano* **2017**, *11*, 1189; b) G. Niu, H. Yu, J. Li, D. Wang, L. Wang, *Nano Energy* **2016**, *27*, 87.
- [20] H. Okamoto, *J. Phase Equilib. Diffus.* **2016**, *37*, 246.
- [21] A. W. Adamson, A. P. Gast, *Physical Chemistry of Surfaces*, Interscience Publishers, New York **1967**, p. 15.
- [22] a) R. L. Smithson, D. J. McClure, D. F. Evans, *Thin Solid Films* **1997**, *307*, 110; b) J. Baumgartner, A. Dey, P. H. Bomans, C. L. Coadou, P. Fratzl, N. A. Sommerdijk, D. Faivre, *Nat. Mater.* **2013**, *12*, 310; c) P. Biswal, S. Stalin, A. Kludze, S. Choudhury, L. A. Archer, *Nano Lett.* **2019**, *19*, 8191; d) Y. S. Zhao, P. Zhan, J. Kim, C. Sun, J. Huang, *ACS Nano* **2010**, *4*, 1630.
- [23] a) J. Xing, X. F. Liu, Q. Zhang, S. T. Ha, Y. W. Yuan, C. Shen, T. C. Sum, Q. Xiong, *Nano Lett.* **2015**, *15*, 4571; b) H. Shim, N. Shin, *J. Phys. Chem. Lett.* **2019**, *10*, 6741.
- [24] B. A. Wacaser, K. A. Dick, J. Johansson, M. T. Borgström, K. Deppert, L. Samuelson, *Adv. Mater.* **2009**, *21*, 153.
- [25] Q. A. Akkerman, G. Raino, M. V. Kovalenko, L. Manna, *Nat. Mater.* **2018**, *17*, 394.
- [26] J. Dean, N. Lange, *Lange's Handbook of Chemistry*, 15th ed, McGraw-Hill, Inc, New York **1999**.
- [27] C. Lan, C. Li, S. Wang, T. He, Z. Zhou, D. Wei, H. Guo, H. Yang, Y. Liu, *J. Mater. Chem. C* **2017**, *5*, 1494.
- [28] C. Lan, Z. Zhou, Z. Zhou, C. Li, L. Shu, L. Shen, D. Li, R. Dong, S. Yip, J. C. Ho, *Nano Res.* **2018**, *11*, 3371.
- [29] O. Lopez-Sanchez, D. Lembke, M. Kayci, A. Radenovic, A. Kis, *Nat. Nanotechnol.* **2013**, *8*, 497.
- [30] Y. Yin, Y. Guo, D. Liu, C. Miao, F. Liu, X. Zhuang, Y. Tan, F. Chen, Z. X. Yang, *Adv. Opt. Mater.* **2022**, *10*, 2102291.